

WATER PROPERTIES

Anomalous low dielectric constant of confined water

L. Fumagalli^{1,2*}, A. Esfandiar³, R. Fabregas^{4,5}, S. Hu^{1,2}, P. Ares^{1,2}, A. Janardanan^{1,2}, Q. Yang^{1,2}, B. Radha^{1,2}, T. Taniguchi⁶, K. Watanabe⁶, G. Gomila^{4,5}, K. S. Novoselov^{1,2}, A. K. Geim^{1,2*}

The dielectric constant ϵ of interfacial water has been predicted to be smaller than that of bulk water ($\epsilon \approx 80$) because the rotational freedom of water dipoles is expected to decrease near surfaces, yet experimental evidence is lacking. We report local capacitance measurements for water confined between two atomically flat walls separated by various distances down to 1 nanometer. Our experiments reveal the presence of an interfacial layer with vanishingly small polarization such that its out-of-plane ϵ is only ~ 2 . The electrically dead layer is found to be two to three molecules thick. These results provide much-needed feedback for theories describing water-mediated surface interactions and the behavior of interfacial water, and show a way to investigate the dielectric properties of other fluids and solids under extreme confinement.

Electric polarizability of interfacial water determines the strength of water-mediated intermolecular forces, which in turn affects phenomena such as surface hydration, ion solvation, molecular transport through nanopores, chemical reactions, and macromolecular assembly (1–3). The dielectric properties of interfacial water have attracted intense interest for many decades (4–7), yet no clear understanding has been reached (8–11). Theoretical (12–14) and experimental studies (15–17) have shown that water exhibits layered structuring near surfaces, which suggests that it may form ordered (ice-like) phases under ambient conditions. Such ordered water is generally expected to exhibit small polarizability because of surface-induced alignment of water molecular dipoles, which are then difficult to reorient by applying an electric field (7–10). Despite these extensive studies, the dielectric constant ϵ of interfacial water and its depth remain essentially unknown because measurements are challenging.

Previous experiments to assess ϵ of interfacial water mostly relied on broadband dielectric spectroscopy applied to large-scale naturally occurring systems such as nanoporous crystals, zeolite powders, and dispersions (4, 5, 10, 18, 19). These systems allow sufficient amounts of interfacial water for carrying out capacitance measurements, but the complex geometries require adjustable parameters and extensive modeling, which results in large and poorly controlled

experimental uncertainties. For example, the extracted values of ϵ depended strongly on assumptions about the interfacial layer thickness. Given the lack of direct probes for measuring the polarizability of interfacial water, most evidence has come from molecular dynamics (MD) simulations, which also involve certain assumptions. These studies generally predict that the polarizability should be reduced by approximately an order of magnitude (7–9), but the quantitative accuracy of these predictions is unclear because the same simulation approach struggles to reproduce the known ϵ for bulk water phases (20).

Here, we used slit-like channels of various heights h that could be filled controllably with water. The channels were incorporated into a capacitance circuit with exceptionally high sensitivity to local changes in dielectric properties, which allowed us to determine the out-of-plane dielectric constant ϵ_{\perp} of the water confined inside. We fabricated our devices by van der Waals assembly (21) of three atomically flat crystals of graphite and hexagonal boron nitride (hBN) following a method reported previously (22–24) (fig. S1). Graphite was used as a bottom layer for the assembly as well as the ground electrode in capacitance measurements (Fig. 1A). Next, a spacer layer was placed on top of graphite, an hBN crystal patterned into parallel stripes. The assembly was completed by placing another hBN crystal on top (Fig. 1, B and C). The spacer determined the channels' height h , and the other two crystals served as top and bottom walls. The reported channels were usually ~ 200 nm wide and several micrometers long. Each of our devices for a given h contained several channels in parallel (Fig. 1), which ensured high reproducibility of our measurements and reduced statistical errors. When required, the channels could be filled with water through a micrometer-size inlet etched in graphite from the back (22, 23) (Fig. 1A).

To probe ϵ of water inside the channels, we used scanning dielectric microscopy based on

electrostatic force detection with an atomic force microscope (AFM), adapting the approach described in (25). Briefly, by applying a low-frequency ac voltage between the AFM tip and the bottom electrode, we could detect the tip-substrate electrostatic force, which translated into the first derivative of the local capacitance dC/dz in the out-of-plane direction z . By raster-scanning the tip, a dC/dz (or “dielectric”) image was acquired, from which local dielectric properties could be reconstructed (24). The device design allowed the AFM tip to be fully isolated from water inside the channels and to operate in a dry atmosphere. Note that the use of hBN is essential for these experiments. First, hBN is highly insulating, which allows the electric field generated by the AFM tip to reach the subsurface water without being screened. It is also highly beneficial to have hBN as the side walls (spacers) because this material provides a straightforward reference for comparison between the dielectric properties of hBN ($\epsilon_{\perp} \approx 3.5$) (26) and the nearby water of the same thickness (Fig. 1C). As shown below, the latter arrangement yielded an unambiguous dielectric contrast, revealing that ϵ of confined water strongly changes with decreasing h independently of the modeling.

Unlike the previous reports (22, 23), we chose to use relatively thin (30 to 80 nm) top crystals, which allowed us not only to reach closer to the subsurface water but also to ensure that the channels were fully filled during the capacitance measurements (see below) (fig. S2) (24). When there was no water inside, the top hBN exhibited notable sagging (22) (Fig. 1B). In Fig. 1, E to G, we show AFM topographic images for representative devices with $h \approx 10$ nm, 3.8 nm, and 1.4 nm, respectively, under dry conditions. All devices exhibited some sagging, the extent of which depended on the thickness of the top hBN (22) (black curves in Fig. 1, H to J). We used the areas that were not covered by the top hBN layer (cyan curves) to determine the channel heights h from the same images. Such initial imaging, as well as dielectric imaging after filling the channels, was carried out at low relative humidity (below 3%) and at room temperature.

Figure 2, A to C, shows AFM topographic images for the same three devices and the same scan areas as in Fig. 1, E to G, but after filling the channels with water, which was done by exposing the backside of our devices to deionized water (22) (Fig. 1A). After the channels were filled, the adhesion between the side and top walls decreased and the sagging diminished (Fig. 1C). The top hBN layer covering water-filled channels became straight with little topographic contrast remaining, independently of h (red curves in Fig. 1, H to J). The corresponding dielectric images for the discussed devices after their filling are shown in Fig. 2, D to F. They show very strong contrast that reverses with decreasing h . For the 10-nm channels, the red regions containing subsurface water indicate ϵ_{\perp} greater than that of hBN, as expected (Fig. 2, D and G, red). For the 3.8-nm-thick water, the dielectric contrast disappeared (Fig. 2, E and G, cyan), whereas the

¹School of Physics and Astronomy, University of Manchester, Manchester M13 9PL, UK. ²National Graphene Institute, University of Manchester, Manchester M13 9PL, UK.

³Department of Physics, Sharif University of Technology, P.O. Box 11155-9161, Tehran, Iran. ⁴Departament d'Electrònica, Universitat de Barcelona, C/ Martí i Franquès 1, 08028 Barcelona, Spain. ⁵Institut de Bioenginyeria de Catalunya, Barcelona Institute of Science and Technology, C/ Baldori i Reixac 15-21, 08028 Barcelona, Spain. ⁶National Institute for Materials Science, 1-1 Namiki, Tsukuba 305-0044, Japan.

*Corresponding author. Email: laura.fumagalli@manchester.ac.uk (L.F.); geim@manchester.ac.uk (A.K.G.)

1.4-nm-thick water exhibited the opposite, negative contrast (Fig. 2, F and G, blue). The images show that the polarizability of confined water strongly depends on its thickness h and reaches values less than that of hBN with its already

modest $\epsilon_{\perp} \approx 3.5$. As mentioned above, a reduction in ϵ_{\perp} for strongly confined water is generally expected from atomistic simulations (7–9), but the observed decrease is much stronger than predicted ($\epsilon_{\perp} \approx 10$) or commonly assumed (24).

To quantify the measured local capacitance and find ϵ_{\perp} for different water thicknesses, we used a three-dimensional electrostatic model that takes into account the specific geometry of the measured devices and the AFM tips chosen (24)

Fig. 1. Experimental setup for dielectric imaging.

(A) Schematic illustration. The top layer and side walls made of hBN are shown in light blue; graphite serving as the ground electrode is in black. The three-layer assembly covers an opening in a silicon nitride membrane (light brown). The channels are filled with water from the back. The AFM tip served as the top electrode and was kept in a dry nitrogen atmosphere.

(B and C) Cross-sectional schematics before (B) and after (C) filling the channels with water (not to scale). (D) Three-dimensional topography image of one of our devices. (E to G) AFM topography of the sagged top hBN for devices with different

values of h before filling them with water. Scale bars, 500 nm. (H to J) Corresponding topography profiles for the top layer (black) and the part not covered by hBN (cyan) as indicated by color-coded lines in (D). Red curves: Same after filling with water.

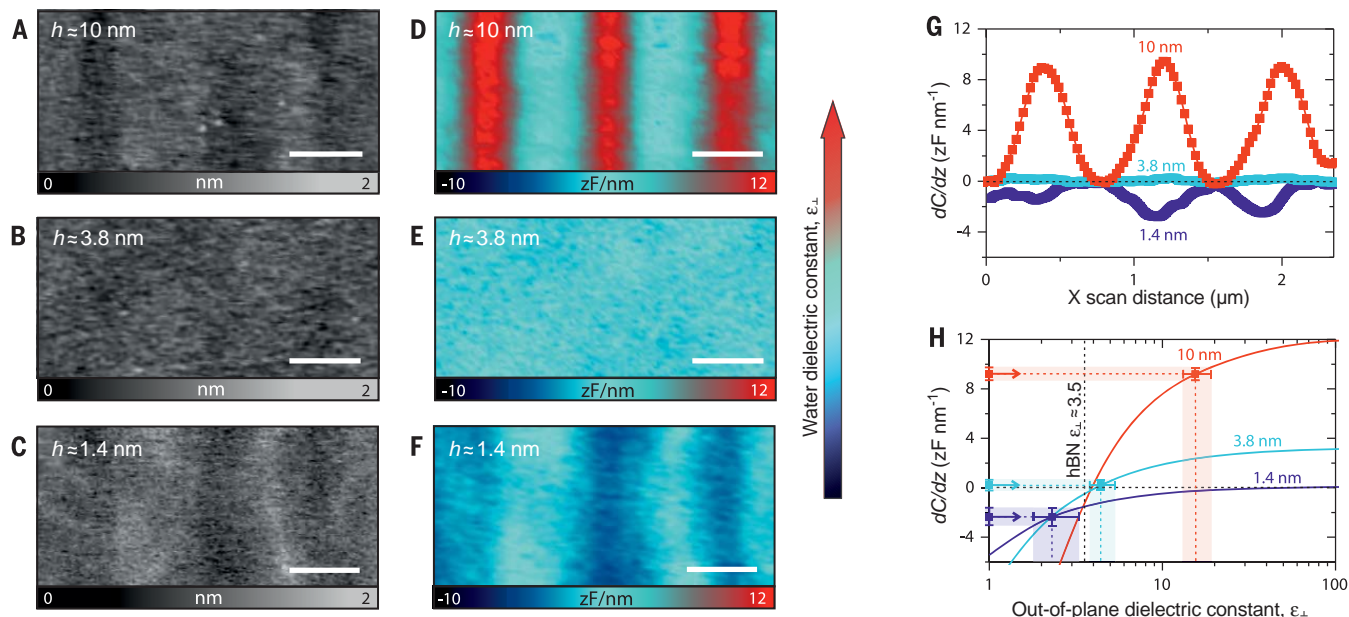
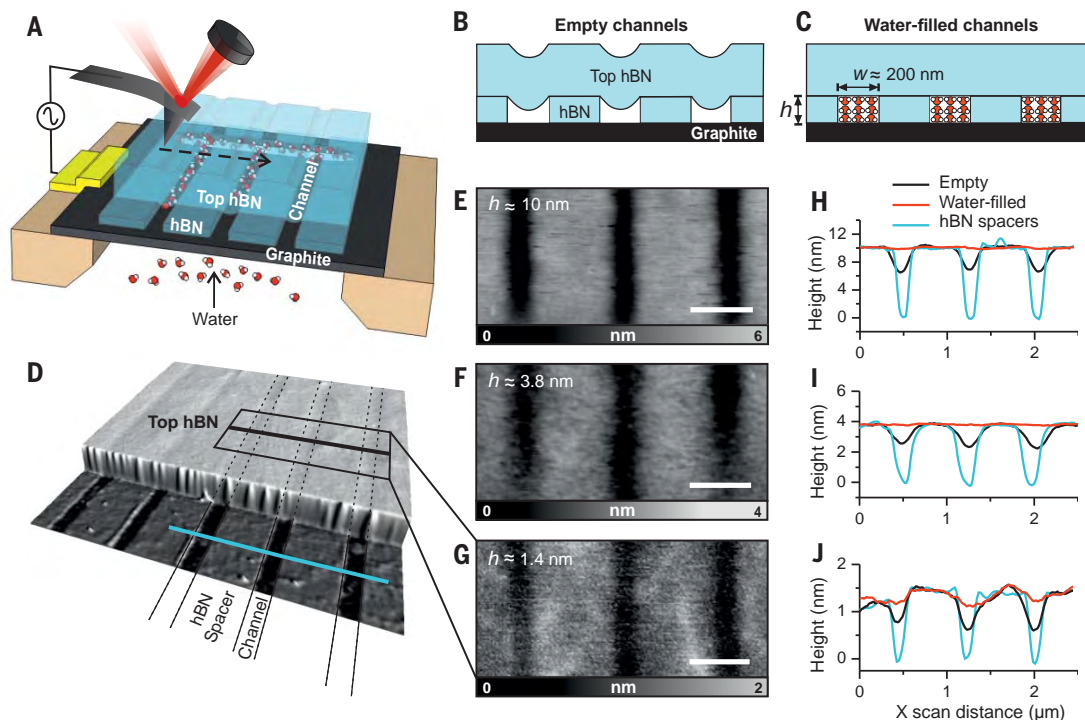


Fig. 2. Dielectric imaging of confined water. (A to C) Topographic images of the three devices in Fig. 1 after filling them with water. Scale bars, 500 nm. (D to F) Corresponding dC/dz images obtained by applying a tip voltage of 4 V at 1 kHz (other voltages and frequencies down to 300 Hz yielded similar images). Commercial cantilevers with tip radii of 100 to 200 nm were used to maximize the imaging sensitivity (24). (G) Averaged

dielectric profiles across the channels in (D) to (F). (H) Simulated dC/dz curves as a function of ϵ_{\perp} for the known geometries of the three studied devices (shown are the peak values in the middle of the channels). Symbols are the measured values of dC/dz from (G). Their positions along the x axis are adjusted to match the calculated curves. Bars and light-shaded regions denote standard errors as defined in (24).

(figs. S3 and S4). The model allows numerical calculation of dC/dz as a function of ϵ_{\perp} for a dielectric material inside the channels. Figure 2H shows the resulting curves for the three studied devices in Fig. 2, A to C. By projecting the measured capacitive signals (symbols on the y axis of Fig. 2H) onto the x axis, we find $\epsilon_{\perp} \approx 15.5$, 4.4, and 2.3 for $h \approx 10$ nm, 3.8 nm, and 1.4 nm, respectively. We emphasize that ϵ_{\perp} is the only unknown in our model, as all the other parameters were determined experimentally. Also, some devices exhibited small (1 to 3 Å) residual sagging in the filled state (see, e.g., Fig. 2, A to C). If not taken into account, this effect could lead to systematic albeit small errors in determining ϵ_{\perp} (by effectively shifting the calculated curves in the y direction). Our calculations included this residual sagging (fig. S5).

We repeated such experiments and their analysis for more than 40 devices with h ranging from ~ 1 to 300 nm. The results are summarized in Fig. 3, which shows the observed ϵ_{\perp} as a function of h . The bulk behavior ($\epsilon_{\perp} \approx 80$) was recovered only for water as thick as ~ 100 nm, which shows that confinement could affect the dielectric properties of even relatively thick water layers (fig. S6). At smaller thicknesses, ϵ_{\perp} evolved approximately linearly with h and approached a limiting value of $\sim 2.1 \pm 0.2$ at $h < 2$ nm, where only a few layers of water could fit inside the channels. Note that the functional dependence in Fig. 3 was found independent of details of our experimental geometries such as thickness of the top hBN layer and the AFM tip radius (fig. S7).

The dielectric constant $\epsilon_{\perp} \approx 2.1$ measured for few-layer water is exceptionally small. Not only is it much smaller than that of bulk water ($\epsilon_{\text{bulk}} \approx 80$) and proton-disordered ice phases such as ordinary ice I_h ($\epsilon \approx 99$) (27, 28), but the value is also smaller than that in low-temperature proton-ordered ices ($\epsilon \approx 3$ to 4) (27). Moreover, the observed ϵ_{\perp} is small even in comparison with the high-frequency dielectric constant ϵ_{∞} resulting from dipolar relaxation [$\epsilon_{\infty} \approx 4$ to 6 for liquid water (29, 30) and $\epsilon_{\infty} \approx 3.2$ for ice I_h (27, 28)]. Nonetheless, $\epsilon_{\perp} \approx 2.1$ lies (as it should) above $\epsilon \approx 1.8$ for water at optical frequencies (27, 30), which is the contribution resulting from the electronic polarization. The above comparison implies that the dipole rotational contribution is completely suppressed, at least in the direction perpendicular to the atomic planes of the confining channels. This result agrees with the MD simulations that find water dipoles to be oriented preferentially parallel to moderately hydrophobic surfaces such as hBN and graphite (12–14). The small ϵ_{\perp} suggests that the hydrogen-bond contribution, which accounts for the unusually large $\epsilon_{\infty} \approx 4$ to

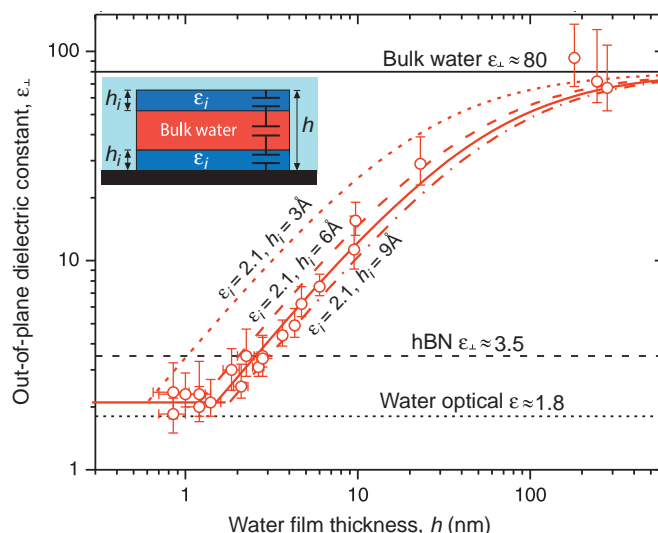


Fig. 3. Dielectric constant of water under strong confinement.

Symbols denote ϵ_{\perp} for water inside channels with different values of h . The y -axis error is the uncertainty in ϵ_{\perp} found from the analysis as described in Fig. 2H. The x -axis error bars show the uncertainty in the water thickness including the residual sagging. Red curves: Calculated $\epsilon_{\perp}(h)$ behavior for the model sketched in the inset. It assumes the presence of a near-surface layer with $\epsilon_i = 2.1$ and thickness h_i , whereas the remainder of the channel contains the ordinary bulk water. Solid curve: Best fit yielding $h_i = 7.4$ Å. The dotted, dashed, and dashed-dotted curves are for $h_i = 3$ Å, 6 Å, and 9 Å, respectively. Horizontal lines: Dielectric constants of bulk water (solid) and hBN (dashed). The dielectric constant of water at optical frequencies (square of its refractive index) is shown by the dotted line. The inset explains our capacitance model with different ϵ values for the bulk and interfacial water.

6 in bulk water (29, 30), is also suppressed. The remaining polarizability can be attributed mostly to the electronic contribution (which is not expected to change under the confinement) plus a small contribution from atomic dipoles, similar to the case of nonassociated liquids (30).

Although the observed ϵ_{\perp} remains anomalously small (< 20) over a wide range of h up to 20 nm (Fig. 3), polarization suppression does not necessarily extend over the entire volume of the confined water. Indeed, the capacitance response can come from both interfacial and inner molecules, effectively averaging their contributions over the channel thickness. To this end, we recall that water near solid surfaces is believed to have a pronounced layered structure that extends ~ 10 Å into the bulk (12–17). Accordingly, the observed dependence $\epsilon_{\perp}(h)$ could be attributed to a cumulative effect from the thin near-surface layer with the low dielectric constant ϵ_i , whereas the rest of the water has the normal, bulk polarizability, $\epsilon_{\text{bulk}} \approx 80$. The overall effect can be described by three capacitors in series (inset of Fig. 3). This model yields the effective $\epsilon_{\perp} = h / [2h_i/\epsilon_i + (h - 2h_i)/\epsilon_{\text{bulk}}]$, where h_i is the thickness of the near-surface layer. Its ϵ_i can be taken as ~ 2.1 in the limit of small h if we assume that the layered structure does not change much with increasing h (13) and is similar at both the graphite and hBN surfaces, as predicted by MD simulations (14). Figure 3 shows that the pro-

posed simple model describes well the experimental data, allowing an estimate for the thickness h_i of interfacial water with the suppressed polarization (24) (fig. S8). Within experimental error, our data yield $h_i \approx 7.5 \pm 1.5$ Å, in agreement with the expected layered structure of water (14–17). In other words, the electrically dead layer extends two to three molecular diameters away from the surface. This result is also consistent with the thickness $h = 1.5$ to 2 nm where the limiting value $\epsilon_{\perp} \approx 2.1$ is reached (see Fig. 3). This h is approximately twice h_i and can be understood as the distance at which the near-surface layers originating from top and bottom walls merge.

We have measured the dielectric constant of water confined at the nanoscale and found it to be anomalously low. Because water exhibits a distinct layered structure near all surfaces, independently of their hydrophilicity (31), it is reasonable to expect that confined and interfacial water have a strongly suppressed ϵ_{\perp} not only near moderately hydrophobic surfaces (such as those studied in this work) but in most cases. Our results are important for better understanding of long-range interactions in biological systems, including those responsible for the stability of macromolecules such as

DNA and proteins, and of the electric double layer that plays a critical role in areas such as electrochemistry and energy storage. The results can also be used to fine-tune parameters in future atomistic simulations of confined water.

REFERENCES AND NOTES

1. J. N. Israelachvili, *Intermolecular and Surface Forces* (Academic Press, ed. 3, 2011).
2. S. Leikin, V. A. Parsegian, D. C. Rau, R. P. Rand, *Annu. Rev. Phys. Chem.* **44**, 369–395 (1993).
3. B. Honig, A. Nicholls, *Science* **268**, 1144–1149 (1995).
4. O. Stern, *Elektrochem. Angew. Phys. Chem.* **30**, 508–516 (1924).
5. B. E. Conway, J. O'M. Bockris, I. A. Ammar, *Trans. Faraday Soc.* **47**, 756–766 (1951).
6. J. B. Hubbard, L. J. Onsager, *J. Chem. Phys.* **67**, 4850–4857 (1977).
7. A. Chandra, *J. Chem. Phys.* **113**, 903–905 (2000).
8. C. Zhang, F. Gygi, G. Galli, *J. Phys. Chem. Lett.* **4**, 2477–2481 (2013).
9. A. Schlaich, E. W. Knapp, R. R. Netz, *Phys. Rev. Lett.* **117**, 048001 (2016).
10. D. Ben-Yaakov, D. Andelman, R. Podgornik, *J. Chem. Phys.* **134**, 074705 (2011).
11. D. J. Bonhuis, R. R. Netz, *Langmuir* **28**, 16049–16059 (2012).
12. C. Y. Lee, J. A. McCammon, P. J. Rossky, *J. Chem. Phys.* **80**, 4448–4455 (1984).
13. G. Cicero, J. C. Grossman, E. Schwegler, F. Gygi, G. Galli, *J. Am. Chem. Soc.* **130**, 1871–1878 (2008).
14. G. Tocci, L. Joly, A. Michaelides, *Nano Lett.* **14**, 6872–6877 (2014).
15. J. N. Israelachvili, R. M. Pashley, *Nature* **306**, 249–250 (1983).
16. M. F. Toney et al., *Nature* **368**, 444–446 (1994).
17. J.-J. Velasco-Velez et al., *Science* **346**, 831–834 (2014).

18. H.-B. Cui *et al.*, *Angew. Chem. Int. Ed.* **44**, 6508–6512 (2005).
19. A. R. Haidar, A. K. Jonscher, *J. Chem. Soc. Faraday Trans. I* **82**, 3535–3551 (1986).
20. J. L. Aragonés, L. G. MacDowell, C. Vega, *J. Phys. Chem. A* **115**, 5745–5758 (2011).
21. A. K. Geim, I. V. Grigorieva, *Nature* **499**, 419–425 (2013).
22. B. Radha *et al.*, *Nature* **538**, 222–225 (2016).
23. A. Esfandiar *et al.*, *Science* **358**, 511–513 (2017).
24. See supplementary materials.
25. L. Fumagalli, D. Esteban-Ferrer, A. Cuervo, J. L. Carrascosa, G. Gomila, *Nat. Mater.* **11**, 808–816 (2012).
26. K. K. Kim *et al.*, *ACS Nano* **6**, 8583–8590 (2012).
27. V. F. Petrenko, R. W. Whitworth, *Physics of Ice* (Oxford Univ. Press, 1999).
28. G. P. Johari, *Contemp. Phys.* **22**, 613–642 (1981).
29. N. E. Hill, *Trans. Faraday Soc.* **59**, 344–346 (1963).
30. N. E. Hill, W. E. Vaughan, A. H. Price, M. Davies, *Dielectric Properties and Molecular Behaviour* (Van Nostrand Reinhold, 1969).
31. O. Björneholm *et al.*, *Chem. Rev.* **116**, 7698–7726 (2016).

ACKNOWLEDGMENTS

We thank N. Walet, P. Carbone, L. Lue, and A. Michaelides for useful discussions. **Funding:** Supported by the Engineering and Physical Sciences Research Council, Lloyd's Register Foundation, Graphene Flagship, European Research Council, and Royal Society. G.G. acknowledges support from Ministerio de Industria, Economía y Competitividad (MINECO, grant TEC2016-79156-P) and ICREA Academia Award. **Author contributions:** L.F. proposed and directed the research with help from A.K.G. and K.S.N.; A.E. fabricated most of the devices with contributions from S.H., A.J., Q.Y., and B.R.; L.F. carried out experiments and data analysis; P.A. helped with image acquisition and processing; R.F., G.G.,

and L.F. implemented finite-element numerical calculations; T.T. and K.W. provided hBN; L.F. and A.K.G. wrote the manuscript; and all authors contributed to discussions. **Competing interests:** We declare no such interests. **Data and materials availability:** All data needed to evaluate the conclusions in the paper are present in the paper and supplementary materials.

SUPPLEMENTARY MATERIALS

www.sciencemag.org/content/360/6395/1339/suppl/DC1
Materials and Methods
Supplementary Text
Figs. S1 to S8
References (32–45)
24 February 2018; accepted 3 May 2018
10.1126/science.aat4191